INTERNATIONAL JOURNAL OF NUMERICAL MODELLING: ELECTRONIC NETWORKS, DEVICES AND FIELDS
Int. J. Numer. Model. 2005; **18**:327–340
Published online 30 June 2005 in Wiley InterScience (www.interscience.wiley.com). DOI: 10.1002/jnm.581

Efficient three-dimensional parallel simulations of PHEMTs

A. J. García-Loureiro[1,*,†], K. Kalna[2,‡] and A. Asenov[2]

[1] *Department of Electronics and Computer Science, Universidad de Santiago de Compostela, Campus Sur, 15782 Santiago de Compostela, Spain*
[2] *Device Modelling Group, Department of Electronics and Electrical Engineering, University of Glasgow, Glasgow, G12 8LT, Scotland, U.K.*

SUMMARY

An efficient 3D semiconductor device simulator is presented for a memory distributed multiprocessor environment using the drift–diffusion (D–D) approach for carrier transport. The current continuity equation and the Poisson equation, required to be solved iteratively in the D–D approach, are discretized using a finite element method (FEM) on an unstructured tetrahedral mesh. Parallel algorithms are employed to speed up the solution. The simulator has been applied to study a pseudomorphic high electron mobility transistor (PHEMT). We have carried out a careful calibration against experimental *I–V* characteristics of the 120 nm PHEMT achieving an excellent agreement. A simplification of the device buffer, which effectively reduces the mesh size, is investigated in order to speed up the simulations. The 3D device FEM simulator has achieved almost a linear parallel scalability for up to eight processors. Copyright © 2005 John Wiley & Sons, Ltd.

KEY WORDS: 3D simulations; drift–diffusion; parallel scalability; domain decomposition; HEMT

1. INTRODUCTION

High electron mobility transistors (HEMTs) used for RF applications have been aggressively shrunk to gate lengths approaching nanometre dimensions [1], in order to attain operating frequencies up to 560 GHz. At this scale, random variations in doping or ternary alloy composition may induce parameter fluctuations and can significantly degrade the RF performance of multifinger devices. To account for these effects the 2D simulations (which neglect a width of the devices) have to be replaced by full 3D simulations which can handle random dopants and material variations. For instance, the device doping cannot be considered anymore continuous and its atomistic nature should be taken into account [2]. Another

*Correspondence to: A. J. García-Loureiro, Department of Electronics and Computer Science, Universidad de Santiago de Compostela, Campus Sur, 15782 Santiago de Compostela, Spain.
†E-mail: antonio@dec.usc.es
‡E-mail: kalna@elec.gla.ac.uk

Contract/grant sponsor: Spanish Government (CICYT); contract/grant number: TIN 2004-07797-C02

Received 16 November 2004
Revised 30 March 2005
Accepted 28 April 2005

Copyright © 2005 John Wiley & Sons, Ltd.

phenomenon, which could affect particularly fast HEMTs with InGaAs channel, is the variation of the content in ternary alloys which may occur in the channel region.

Development of adequate 3D simulators for HEMTs is therefore essential for a better understanding of the impact of parameter fluctuations on device characteristics for design optimization [3]. Unfortunately, 3D device simulators require large amounts of memory and high power CPUs due to the fact that calculation time increases exponentially with the number of discretization nodes in the simulation domain. In this work, we present an efficient 3D parallel device simulator which utilizes the finite element method (FEM) within the drift–diffusion (D–D) approximation to semiconductor transport and is suitable for the statistical simulation of intrinsic parameter variations. The properties of the resulting large linear systems necessitates the development of adequate parallel solvers since traditional methods, such as incomplete factorizations, are very inefficient. Therefore, we have studied various domain decomposition methods which may be employed to solve the linear systems in parallel [4].

The simulator has been developed for distributed-memory computers [5]. It employs a multiple instruction-multiple data strategy (MIMD) under the single program-multiple data paradigm (SPMD) which is achieved by using the message passing interface (MPI) standard library [6]. We have chosen the MPI library due to its availability on many computer systems which guarantees the portability of the code [7]. The capabilities of the 3D device simulator have been tested in comparison with measured characteristics of a real 120 nm pseudomorphic HEMT (PHEMT) with a low indium content channel of 0.2, fabricated and characterized in the Nanoelectronics Research Centre at the University of Glasgow [8].

The paper is organized as follows. Section 2 describes the main characteristics of our 3D simulator. Section 3 presents the domain decomposition methods which have been used to solve the linear systems. Results obtained from the simulation of the 120 nm PHEMT are presented in Section 4 while conclusions are drawn up in Section 5.

2. EQUATIONS AND DISCRETIZATION

The object of the semiconductor device simulations is to relate electrical characteristics of the semiconductor devices to their physical and geometrical parameters [9, 10]. Our parallel 3D device simulator, based on the D–D approximation [9] to the Boltzmann transport equation [9], uses the FEM on an unstructured tetrahedral mesh allowing an accurate description of the device geometry mainly around the gate and recesses.

The D–D approach has to be simplified as much as possible to reduce the computational time. Therefore, because the HEMTs are n-type majority carrier devices far from a breakdown, we can neglect the hole continuity equation, $\mathrm{div}(J_p) = -qR$, which describes the transport of holes. In this case, the D–D system of semiconductor equations reduces into the following two equations:

$$\mathrm{div}(\varepsilon \nabla \psi) = q(-n + N_{\mathrm{D}}^{+}) \tag{1}$$

$$\mathrm{div}(J_n) = 0 \tag{2}$$

These equations are scaled using a procedure described in Reference [10]. The scaled Poisson equation can be expressed as

$$\lambda^2 \nabla^2 \psi = (n - C), \quad x \in \Omega \tag{3}$$

Copyright © 2005 John Wiley & Sons, Ltd.

where the parameter λ is defined as $\lambda = \sqrt{\varepsilon V_T / q C_0 l_0}$, ε is the dielectric constant of the material, V_T is the thermal voltage, q is the electron charge, C_0 and l_0 are the scaled values for concentration and length, respectively. This equation is subjected to the following boundary conditions:

$$\left.\frac{\partial \Psi}{\partial v}\right|_{\partial\Omega_N} = 0 \tag{4}$$

$$\Psi|_{\partial\Omega_{D1}} = \Psi_b + V(t)_{D1} \tag{5}$$

$$\Psi|_{\partial\Omega_{D2}} = \Psi_b - \Psi_S + V(t)_{D2} \tag{6}$$

where the boundary $\partial\Omega$ of the simulation domain Ω splits into Neumann segments $\partial\Omega_N$ and Dirichlet segments $\partial\Omega_D$. Dirichlet segments are divided in two parts: D1 are the segments corresponding to the Ohmic contact (source and drain contacts), and D2 are the segments for the Schottky contact (gate contact). $V(t)$ is the externally applied bias, which may be different for each of the contacts, Ψ_b is the built-in potential, and Ψ_S is the Schottky barrier height.

The FEM is applied to discretize Equations (3)–(6), using tetrahedral elements. At the pre-processing the solution domain representing the HEMT is triangulated into tetrahedrons. The triangulation is carried out using the QMG program [11] and reflects the specific features of the HEMT geometry including the T-shape gate and the gate recesses. The result is an unstructured mesh illustrated in Figure 1. More nodes are close to the interface between different regions of the transistor and around the gate recess because there the gradients of the electric field and the electron concentration are the greatest.

The solution domain is then partitioned into subdomains, each assigned to an individual processor using the program METIS [12]. The same program is subsequently used to achieve an improved ordering of the nodes of each subdomain. Since various computations have to be performed on the separate elements of the mesh at the matrix assembly stage, it is advantageous to transform the elements into a reference element T_m with vertices $(0,0,0), (1,0,0), (0,1,0)$ and $(0,0,1)$ to use the following co-ordinate transformation:

$$x = (x_0, x_1, x_2), \quad \xi = (\xi_0, \xi_1, \xi_2), \quad x = x(\xi) \tag{7}$$

Then the FEM based on tetrahedral element is applied, using the Ritz–Galerkin approximation. In this case, the shape functions are build from piecewise linear functions [13]. This leads to following weak formulation of the Poisson equation:

$$\begin{aligned} &\lambda^2 \sum_{j=1}^{K} \int_{\Omega_e} (\nabla \widehat{\varphi}_j)^t \nabla \widehat{\varphi}_i |J_e| \, \mathrm{d}\Omega_e \psi_j \\ &+ \sum_{j=1}^{K} \int_{\Omega_e} (n_j - C_j) \widehat{\varphi}_j \widehat{\varphi}_i |J_e| \, \mathrm{d}\Omega_e = 0 \quad \forall i = 1, \ldots, K \end{aligned} \tag{8}$$

where K is the number of vertices in $\bar{\Omega}$, and $\widehat{\varphi}_i$ and $\widehat{\varphi}_j$ are the shape functions for the master tetrahedron Ω_e at the vertex P_j and P_i.

The discretization of the current equation (2) requires particular care and calls for the use of special techniques such as the Scharfetter–Gummel scheme [10].

Copyright © 2005 John Wiley & Sons, Ltd.

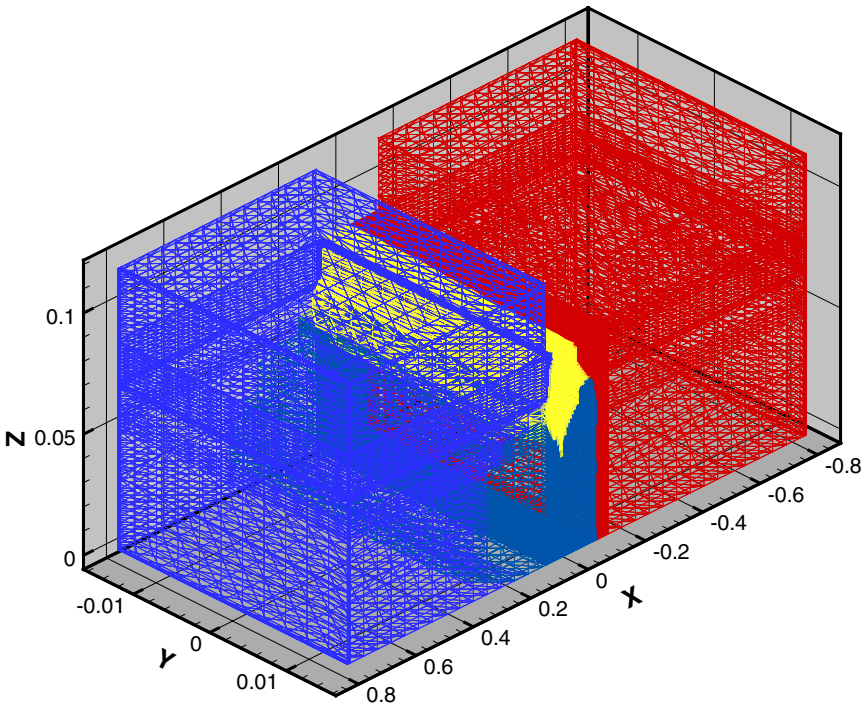

Figure 1. Tetrahedral mesh of the 120 nm PHEMT divided in three subdomains.

If J_e denotes the Jacobian of the map $x = x(\xi)$ of T element to the reference element T_{m}; $B_T(\Delta\psi_{\mathrm{D}}) = \mathrm{diag}(B(\psi_{\mathrm{D}}(P_0) - \psi_{\mathrm{D}}(P_1)), \ldots)$, where B is the Bernoulli function, and P_i, $i = 0, \ldots, n$ are the vertices of the reference element T_{m}; and G_{m} is the centre of gravity of T_{m}, and $x_{G_T} = x(G_{\mathrm{m}})$ the image of G_{m} in the element T, we can write:

$$J_{n,G_T} = \mu_n n_{ien,G_T} \mathrm{e}^{\psi_{\mathrm{D}}(P_0)} J_e^{-t} B_T(\Delta\psi_{\mathrm{D}}) J_e^t \nabla \mathrm{e}^{-\phi_n}|_{\mathrm{D}} \tag{9}$$

which correspond to the value of the current density inside an element. The variables marked with the subscript D refer to the values of the discretized variable in the nodes of the mesh. Using the FEM, the following discretized equations are obtained:

$$\sum_{\Omega_e} \int_{\Omega_e} \mu_{n,G_e} n_{ien_\triangle,G_T} \exp(\psi_\triangle(P_0)) \nabla\varphi_j J_e^{-t} B_T(\psi_\triangle) J_e^t \nabla(\exp(-\phi_{n_i})) \nabla\varphi_i \, \mathrm{d}\Omega_e = 0 \quad \forall i = 1, \ldots, K \tag{10}$$

Applying Fermi–Dirac statistics, the electron concentration in a single parabolic conduction band approximation can be obtained as

$$n = N_c F_{1/2}(\eta_c) \tag{11}$$

where N_c is the effective density of states in the conduction band E_c, $F_{1/2}$ is the Fermi–Dirac integral of order $\frac{1}{2}$, and η_c is given by

$$\eta_c = \frac{E_{fn} - E_c}{kT} \tag{12}$$

Copyright © 2005 John Wiley & Sons, Ltd.

Note that η_c depends on the electrostatic potential and the electron quasi-Fermi potential, E_{fn}. Since these variables are the unknowns in the numerical implementation of the model, an self-consistent solution process must be established in order to guarantee coherent results.

3. PARALLELIZATION

In order to deal with non-linearities in Equations (9) and (11) the Poisson and electron continuity equations are decoupled using Gummel methods and linearized using Newton's algorithm. All these algorithms are implemented fully in parallel manner. The linear system associated with the Poisson equation is well conditioned and easy to solve. However, the linear system associated with the electron continuity equation causes significant difficulties.

In our parallel implementation, the above linear systems are solved using domain decomposition technique [14]. The solution domain Ω is partitioned in p subdomains Ω_i as

$$\Omega = \bigcup_{i=1}^{p} \Omega_i \tag{13}$$

and the domain decomposition methods attempt to solve the problem on the entire domain Ω by concurrent solutions on each subdomain Ω_i.

A subdomain of the physical solution domain is illustrated in Figure 2. Each node belonging to a subdomain is an unknown of the whole problem. It is important to distinguish between three types of unknowns: (i) interior nodes are those that are coupled only with local nodes, (ii) local interface nodes are those coupled with external nodes as well as local nodes and (iii) external interface nodes which are those nodes in other subdomains coupled with local nodes. We label the nodes according to their subdomains, first the internal nodes and then the interface nodes. As a result, the linear system associated with the problem has the following structure:

$$\begin{pmatrix} B_1 & & & & & E_1 \\ & B_2 & & & & E_2 \\ & & \cdot & & & \\ & & & \cdot & & \\ & & & & B_p & E_p \\ F_1 & F_2 & & & F_p & C \end{pmatrix} \begin{pmatrix} x_1 \\ x_2 \\ \cdot \\ \cdot \\ x_s \\ y \end{pmatrix} = \begin{pmatrix} f_1 \\ f_2 \\ \cdot \\ \cdot \\ f_s \\ g \end{pmatrix} \tag{14}$$

where for the subdomain Ω_i, y represents the vector of all interface unknowns, B_i represents the equations of internal nodes, C the equations of interface nodes, E_i the subdomain to the interface coupling seen from the subdomains and F_i represents the interface to the subdomain coupling seen from the interface nodes.

A partitioning of the mesh into subdomains is performed using the program METIS. The same program was subsequently used to relabel the nodes in the subdomains in order to obtain a more suitable rearrangement to reduce the bandwidth of the matrix. The PSPARSLIB [15], parallel sparse iterative solvers library, has been used to solve the linear system (14). A great advantage of this library is its optimization for various powerful multicomputers. The best result

Copyright © 2005 John Wiley & Sons, Ltd.

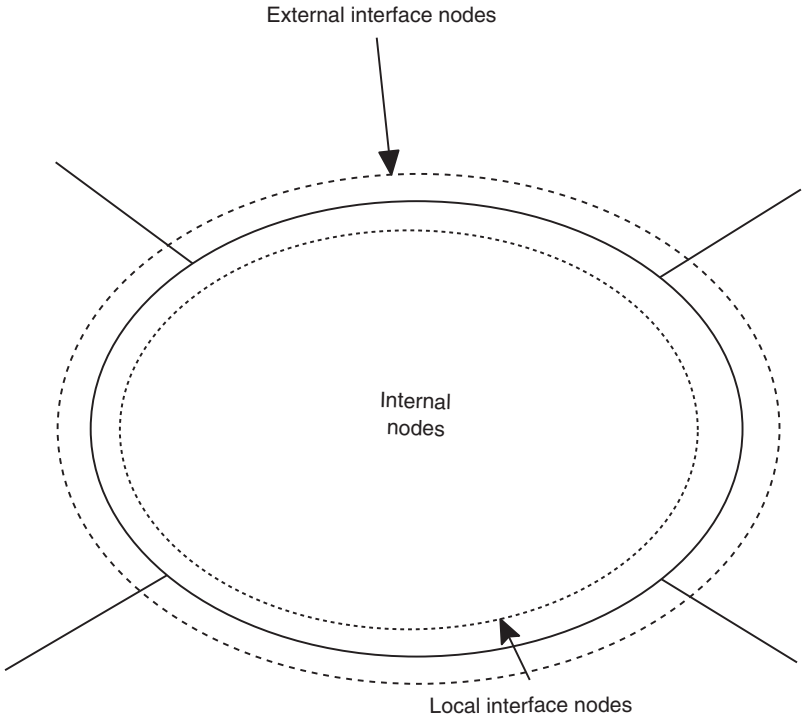

Figure 2. Nodes in a subdomain.

from many domain decomposition techniques supported within this library was obtained when using the additive Schwarz and Schur complement techniques.

3.1. Additive Schwarz technique

The additive Schwarz technique used to solve the linearized systems of equations is similar to a block-Jacobi iteration and consists of updating all the new components from the same residual. The basic additive Schwarz iteration can be described as follows:

1. Obtain $y_{i,\text{ext}}$.
2. Compute a local residual $r_i = (b - Ax)_i$.
3. Solve $A_i\delta_i = r_i$.
4. Update solution $x_i = x_i + \delta_i$.

To solve the linear system $A_i\delta_i = r_i$, a standard ILUT preconditioner combined with GMRES for the solver associated with the blocks is used [4].

3.2. Schur complement techniques

Schur complement techniques refer to methods which iterate on the interface unknowns only, implicitly using the internal unknowns as intermediate variables.

Copyright © 2005 John Wiley & Sons, Ltd.

Consider the linear system (14), for the subdomain Ω_i described as

$$\begin{pmatrix} B_i & E_i \\ F_i & C_i \end{pmatrix} \begin{pmatrix} x_i \\ y_i \end{pmatrix} = \begin{pmatrix} f_i \\ g_i \end{pmatrix} \tag{15}$$

in which B is assumed to be non-singular. From the first equation of (15) the unknown x can be expressed as

$$x = B^{-1}(f - Ey) \tag{16}$$

Upon substituting this into the second equation of (15), the following reduced system is obtained:

$$(C - FB^{-1}E)y = g - FB^{-1}f \tag{17}$$

where the matrix $C - FB^{-1}E = S$ is called the Schur complement matrix associated with the y variable. If this system can be solved, all the interface variables y will become available, and then the remaining unknowns can be computed using Equation (16). Because of the particular structure of this matrix, the global linear system can be decoupled into p separate systems. The parallelism arises from this natural decoupling.

The program has been parallelized and tested on an IBM Netfinity 5500 parallel computer using the message-passing standard library MPI.

4. RESULTS AND DISCUSSION

We have applied the 3D D–D parallel device simulator to model the behaviour of a 120 nm PHEMT fabricated and measured at Glasgow University [16]. The flexible tetrahedral finite element mesh and parallelism of the simulator are fully exploited to depict the complex geometry of this device and to accurately capture electrostatic effects associated with the gate and the recess geometry (see Figure 3). The structure of the studied 120 nm PHEMT has been modelled using a tetrahedral mesh consisting of 29 012 nodes and 147 682 elements.

The structure of the simulated T gate PHEMT is schematically depicted in Figure 3. The device consists of a 30 nm heavily Si-doped (4×10^{18} cm^{-3}) $n+$ GaAs cap layer; an $Al_{0.3}Ga_{0.7}As$ etchstop layer; a 7×10^{12} cm^{-2} Si delta doped layer on top of a 7 nm $Al_{0.3}Ga_{0.7}As$ spacer layer which separates the delta doping from an 10 nm $In_{0.2}Ga_{0.8}As$ channel. The whole device structure is grown on top of a 500 nm GaAs buffer. The dimensions and doping concentrations in the different layers of the simulated device are collected in Table I.

Figure 4 illustrates the distribution of the electrostatic potential at the zero bias. The critical regions where the potential can change abruptly are around the gate and below the recess regions. Here, the number of nodes has to be very large in order to correctly sample the potential gradients. The corresponding semilogarithmic plot of the electron density, at the zero bias, is shown in Figure 5.

Figures 6 and 7 show the simulated I_D–V_G characteristics at a drain bias of 0.1 and 0.3 V, respectively. The I_D–V_G characteristics directly obtained from the 3D D–D simulator does not include the contact resistance and therefore the drain current is higher than the experimental results at large gate voltages. In order to validate the corresponding intrinsic I_D–V_G characteristics obtained from the 3D D–D simulator we have compared them with carefully calibrated results obtained from ensemble Monte Carlo simulations [8] which for the purpose of

Copyright © 2005 John Wiley & Sons, Ltd.

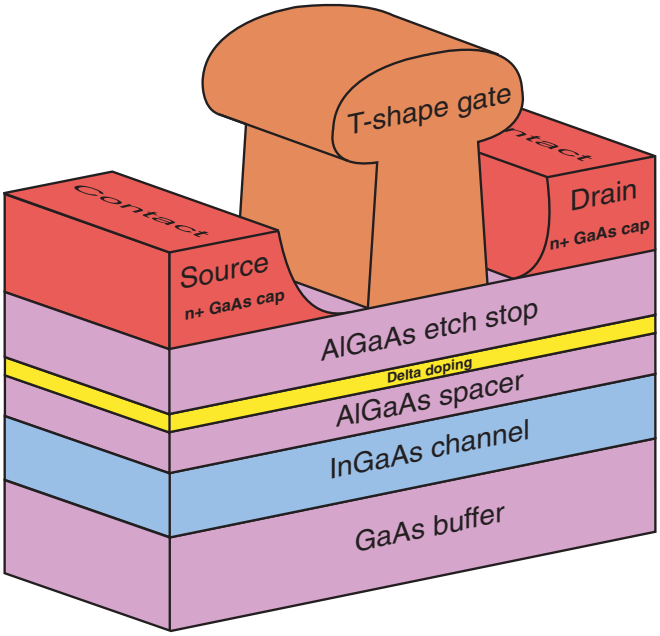

Figure 3. Structure of the PHEMT.

Table I. Dopings and dimensions of PHEMT.

	N_{eff} (cm^{-3})	ΔX (μm)	ΔY (μm)	ΔZ (μm)
Cap layer	4.0×10^{18}	0.690	100.0	0.030
Spacer up	1.0×10^{14}	1.6	100.0	0.017
Delta doping	1.75×10^{19}	1.6	100.0	0.002
Spacer down	1.0×10^{14}	1.6	100.0	0.007
Channel	2.0×10^{14}	1.6	100.0	0.010
Buffer	1.0×10^{14}	1.6	100.0	0.500

this comparison does not include the surface potential pinning at the recess region surface. This allows for a fair comparison since the 3D D–D simulator does not allow at this stage the inclusion of the interface charge. In order to compare intrinsic I–V characteristics obtained directly from any device simulator with experimental data, external resistances of the source and drain have been included at post-processing state [17]. Therefore, both Figures 6 and 7 show also the calibrated Monte Carlo results which include external resistances of the source and drain (3.0 Ω and 2.97 Ω, respectively, obtained experimentally [8]) compared to the experimental measurements. Since the results obtained from the 3D D–D simulator (crosses and open triangles) are in an excellent agreement with the intrinsic Monte Carlo results (open circles) we are confident that they will give the same agreement with the experimental data (full circles) as it is the case for the Monte Carlo results.

Copyright © 2005 John Wiley & Sons, Ltd.

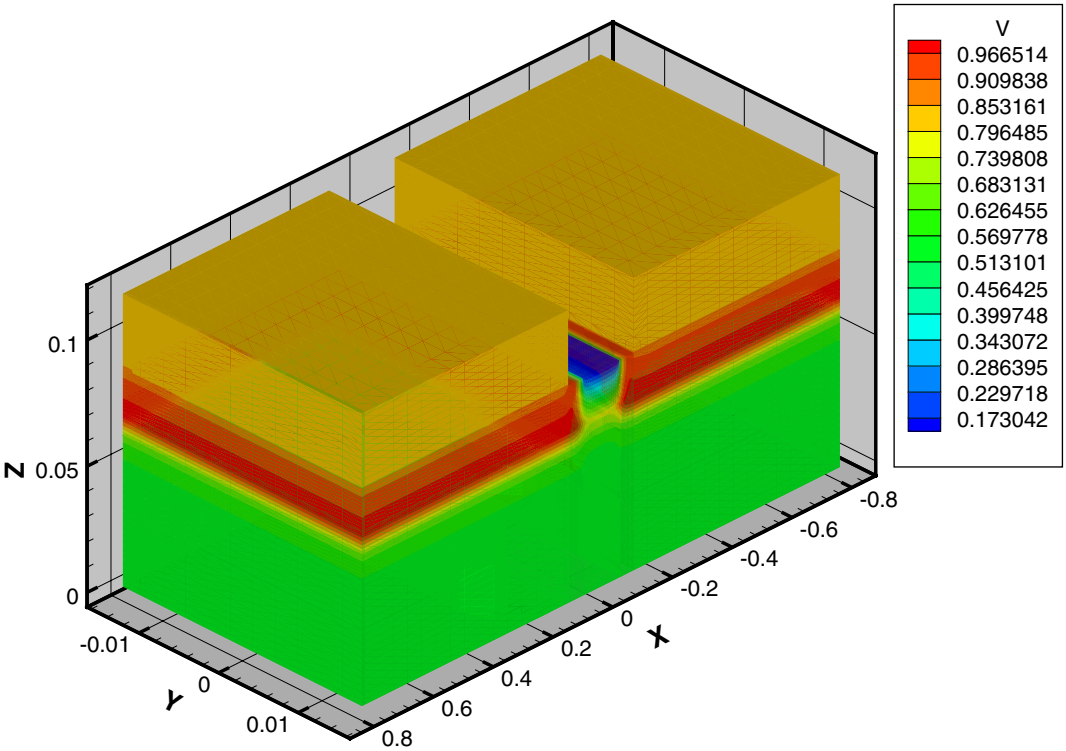

Figure 4. Electrostatic potential at both gate and drain voltages of 0.0 V.

Figures 8 and 9 compare simulations of a large device with the realistic substrate (300 nm) and a simplified device with the shallow substrate (50 nm buffer) against experimental data. The reduction of the device substrate to 50 nm can substantially increases the speed of the simulation. The figures indicate that in the device with reduced substrate the drain current is correctly reproduced above a device pinch-off gate bias but below the pinch-off the drain current is significantly lower than the experimental results. Therefore, a realistic buffer width of 300 nm has to be taken into account to represent properly this part of the characteristics. Figure 8 also illustrates that a simulation of the drain current below the pinch-off at a low drain bias of 0.1 V is very difficult even with the realistic substrate mesh since the resulting current still underestimates the real current by a factor of 3. However, at a drain bias of 0.3, the simulation using the realistic substrate mesh gives an excellent agreement with experimental data even below the pinch-off as demonstrated in Figure 9.

In order to study the scalability of the simulator we have measured the number of MFLOPS (million of floating point operations per second) using a different number of processors on the IBM Netfinity 5500 parallel computer. The results are shown in Figure 10. The parallel performance obtained in the simulations clearly indicates that the 3D D–D simulator has a very good scalability up to eight processors.

Copyright © 2005 John Wiley & Sons, Ltd.

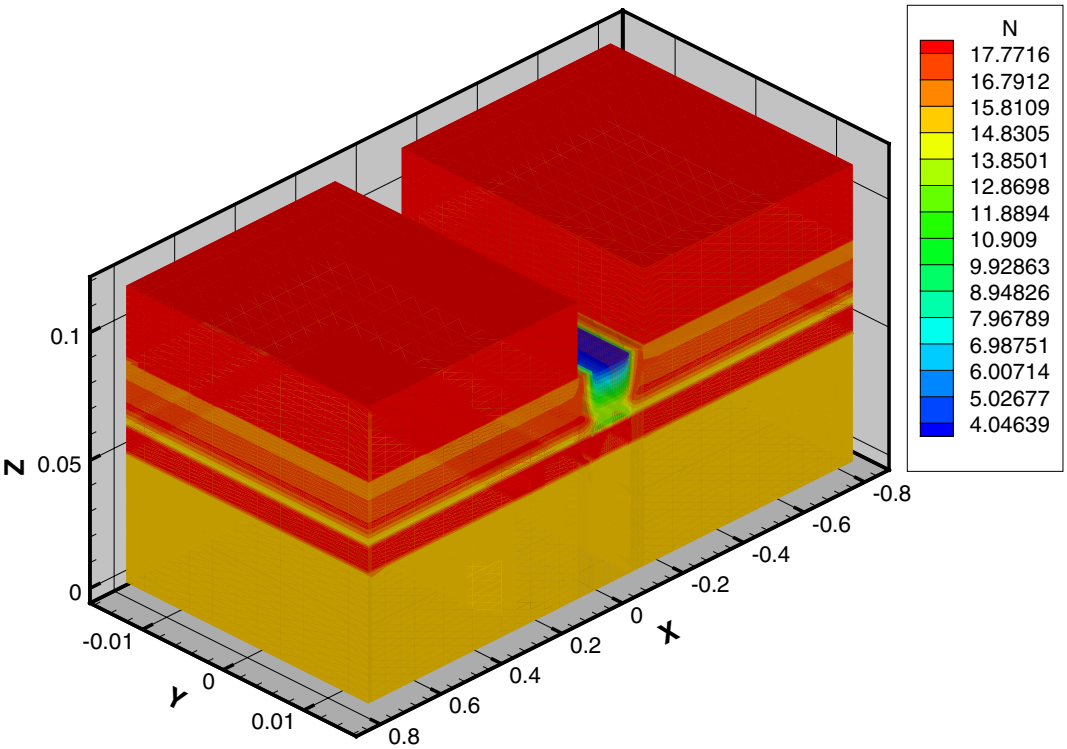

Figure 5. Electron density at both gate and drain voltages of 0.0 V.

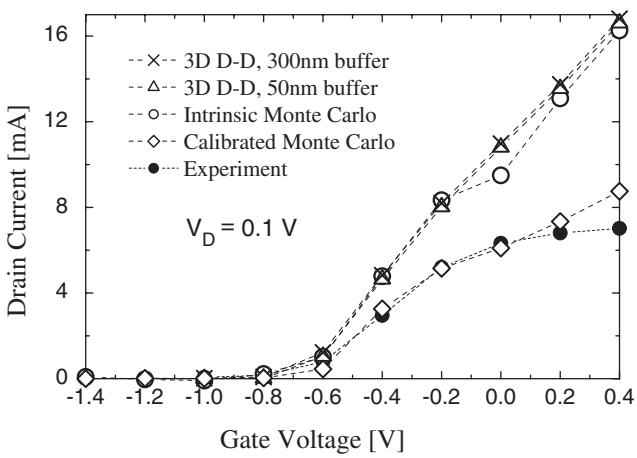

Figure 6. I_D–V_G characteristics at a drain bias of 0.1 V for the 120 nm PHEMT on a linear scale. The buffer approximated by a 50 nm width (open triangles) is compared to a more realistic width of 300 nm (crosses) and to the intrinsic Monte Carlo results (open circles). The calibrated Monte Carlo data (open diamonds) represent the intrinsic results with included external resistances and can be directly compared to experiments (full circles).

Copyright © 2005 John Wiley & Sons, Ltd.

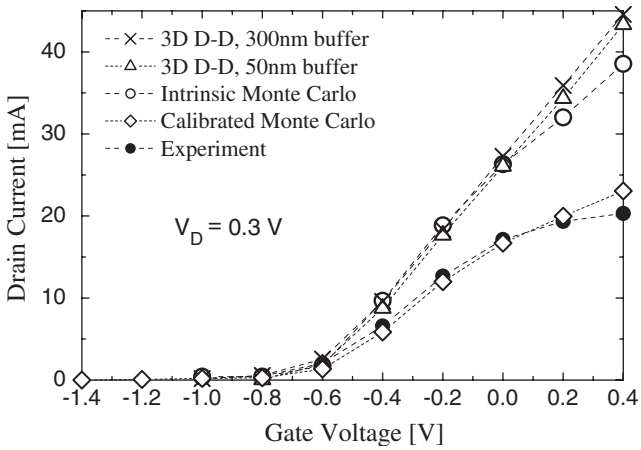

Figure 7. The I_D–V_G characteristics as in Figure 6 but at a drain bias of 0.3 V. Again, results from the 3D D–D parallel device simulator (crosses and open triangles) are compared with intrinsic Monte Carlo data (open circles). The calibrated Monte Carlo data (open diamonds) and experimental data (full circles) are also shown.

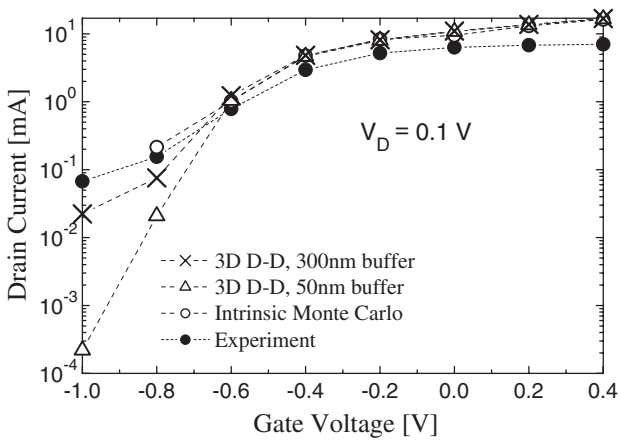

Figure 8. The I_D–V_G characteristics at $V_D = 0.1$ V on a logarithmic scale. The small depth substrate approximation (50 nm buffer) shown by open triangles underestimates the sub pinch-off region when compared to experimental data given by full circles. The realistic substrate mesh (300 nm buffer) shown by crosses gives a much better agreement with experimental results even still underestimates the real current in the sub pinch-off region.

5. CONCLUSIONS

In this work, we have described an efficient 3D device simulator which can be used for statistical investigations of intrinsic parameter fluctuations in compound HEMT. Both the computational and the numerical aspects of the parallel implementation of the simulator has been studied in

Copyright © 2005 John Wiley & Sons, Ltd.

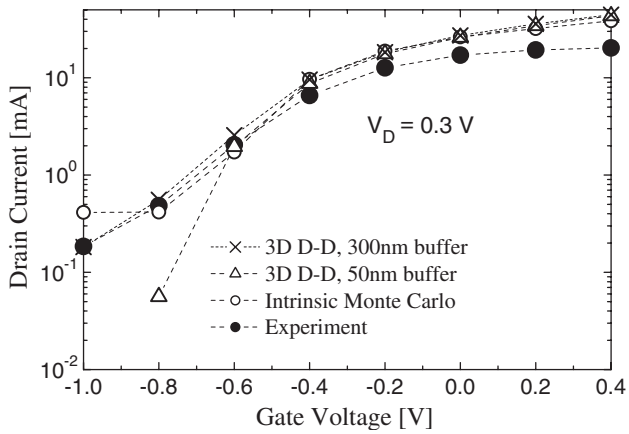

Figure 9. The I_D–V_G characteristics at $V_D = 0.3$ V on a logarithmic scale. The results using the 50 nm buffer approximation (open triangles) are compared with those using the 300 nm buffer realistic substrate (crosses) and with the experimental data given by full circles. The small depth substrate approximation again underestimates the real current by an order of magnitude. However, the realistic depth substrate gives an excellent agreement with experiments.

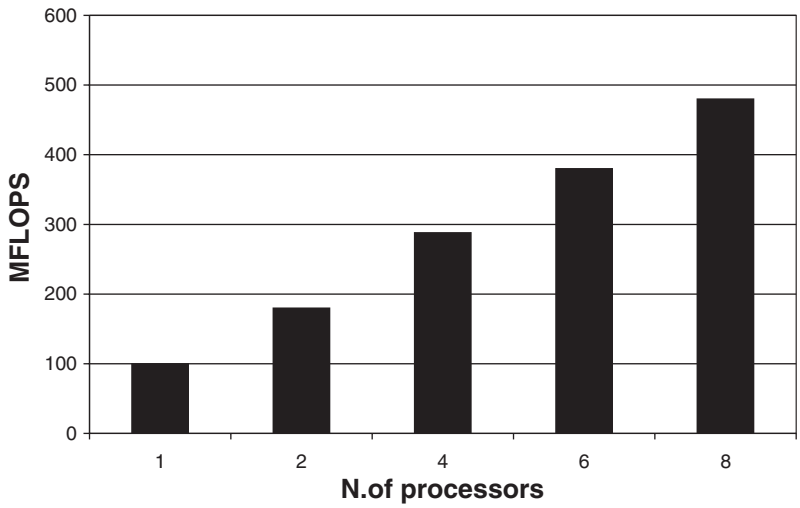

Figure 10. Parallel performance of the 3D D–D simulator.

details. The 3D parallel simulations are essential tool for studying effects of fluctuations, both in doping and in material composition, when these devices are scaled into deep submicron dimensions.

The simulator has been employed to model *I–V* characteristics of the 120 nm gate length PHEMT with a low indium content of 0.2 in the channel. We have demonstrated that the 3D

Copyright © 2005 John Wiley & Sons, Ltd.

parallel D–D device simulator can be accurately calibrated against ensemble Monte Carlo simulations or experimental data. When the thickness of the device substrate is reduced in order to speed up the 3D simulations the resulting drain current remains in excellent agreement with the reference Monte Carlo results above the pinch-off. However, to reproduce the drain current below the pinch-off a realistic buffer depth must be considered.

The simulator has been implemented to run effectively on memory-distributed parallel computers. Furthermore, the parallel implementation which makes the use of the message passing standard libraries (MPI) ensures both excellent portability and scalability. Various solvers of linear systems have been tested with the aim of selecting those that are the best adapted for linear system arising from the discretization of the semiconductor equations. The scalability of the 3D parallel D–D simulator has been found to be practically linear up to eight processors.

ACKNOWLEDGEMENTS

This work was partly supported by the Spanish Government (CICYT) under project TIN 2004-07797-C02 and by the grant of mobility program of Xunta de Galicia to A. J. García Loureiro in Device Modelling Group at the University of Glasgow.

REFERENCES

1. Yamashita Y, Endoh A, Shinohara K, Hikosaka K, Matsui T, Hiyamizu S, Mimura T. Pseudomorphic $In_{0.52}Al_{0.48}As/In_{0.7}Ga_{0.3}As$ HEMTs with an ultrahigh f_t of 562 Ghz. *IEEE Electronic Device Letters* 2002; **23**(10):573–575.
2. Asenov A. Random dopant induced threshold voltage lowering and fluctuations in sub 0.1 μm MOSFETs: a 3D 'Atomistic' simulation study. *IEEE Transactions on Electron Devices* 1998; **45**:2505–2513.
3. Hussain S, Cole E, Snowden CM. Hot-Electron numerical modelling of short gate length pHEMTs applied to novel field plate structures. *International Journal of Numerical Modelling*: *Electronics Networks*, *Devices and Fields* 2003; **16**:15–28.
4. Saad Y. *Iterative Methods for Sparse Linear Systems*. PWS Publishing Co.: Boston, 1996.
5. García-Loureiro AJ, Pena TF, López-González JM, Prat L. Parallel finite element method to solve the 3D Poisson equation and its application to abrupt heterojunction bipolar transistors. *International Journal for Numerical Methods in Engineering* 2000; **49**(5):639–652.
6. Group W, Lusk E, Skjellum A. *Using MPI*. The MIT Press: Boston, 1996.
7. The Message Passing Interface Standard. http://www-unix.mcs.anl.gov/mpi/index.html
8. Kalna K, Roy S, Asenov A, Elgaid K, Thayne I. Scaling of PHEMTs to decanano dimensions. *Solid-State Electronics* 2002; **46**:631–638.
9. Selberherr S. *Analysis and Simulation of Semiconductor Devices*. Springer: Berlin, 1984.
10. Markowich PA. *The Stationary Semiconductor Device Equations*. Springer: Berlin, 1986.
11. Vavasis SA. *QMG 1.1 Reference Manual*. Computer Science Department, Cornell University, 1996.
12. Karypis G, Kumar V. METIS: a software package for partitioning unstructured graphs, partitioning meshes, and computing fill-reducing orderings of sparse matrices, University of Minnesota, 1997.
13. Zienkiewicz OC. *The Finite Element Method*. McGraw-Hill: New York, 1977.
14. Barrett R, Berry M, Chan T, Demmel J, Donato J, Dongarra J, Eijkhout V, Pozo R, Romine C, van der Vorst H. *Templates for the Solution of Linear Systems*: *Building Blocks for Iterative Methods*. SIAM: Philadelphia, 1994.
15. Saad Y, Lo G-C, Kuznetsov S. PSPARSLIB users manual: a portable library of parallel sparse iterative solvers. *Technical Report*, Department of Computer Science, University of Minnesota, 1997.
16. Kalna K, Asenov A, Elgaid K, Thayne I. Scaling of PHEMTs to decanano dimensions. *VLSI Design* 2001; **13**(1–4):435–439.
17. Babiker S, Asenov A, Cameron N, Beaumont SP. A simple approach to include external resistances in the Monte Carlo simulation of MESFETs and HEMTs. *IEEE Transactions on Electron Devices* 1996; **43**: 2032–2034.

Copyright © 2005 John Wiley & Sons, Ltd.

AUTHORS' BIOGRAPHIES

Antonio J. García-Loureiro received the MS degree in Physics from the University of Santiago de Compostela in 1994 and the PhD degree from the University of Santiago de Compostela in 1999. His doctoral research work was on modelling and simulation of InP- and GaAs-based heterojunction bipolar transistors, having developed a 3D parallel numerical simulator for graded and abrupt HBTs. Currently, he is an Assistant Professor in the Department of Electronics and Computer Science at the University of Santiago de Compostela. His current research interests are modelling of bipolar HBTs, HEMTs and MOSFETs using 3D parallel drift–diffusion device simulations.

Karol Kalna was born in Plzen, Czechoslovakia, on 4 December, 1965. He received the MSc degree in Solid State Physics in 1990 and PhD degree in Condensed Matter in 1998, both from Comenius University, Bratislava, Slovakia. In 1994 he joined Institute of Electrical Engineering, Bratislava, Slovakia as a research scientist. In 1994 he was a postgraduate student at UIA University of Antwerp, Belgium and in 1997 he was awarded by a fellowship from Ministry of Flemish Community again at the same university. In 1999 he received a grant from Royal Society to work on quantum cascade lasers at University of Wales, Bangor. Since 1999 he is a research assistant at Device Modelling Group, Department of Electronics & Electrical Engineering, University of Glasgow. His current research interests are modelling of HEMTs and III-V MOSFETs using ensemble Monte Carlo device simulations. The further research interests are 2D carrier transport in semiconductor lasers.

Asen Asenov has 10 years industrial experience as a head of the Process and Device Modelling Group in IME—Sofia, developing one of the first integrated process and device CMOS simulators IMPEDANCE. He was visiting professor at the Physics Department of TU Munich, and is currently a Professor in the Department of Electronics and Electrical Engineering, Glasgow University. As a leader of the Device Modelling Group he has contributed to the development of 2D and 3D device simulators and their application in the design of Si, strained Si and SiGe MOSFETs as well as HEMTs. He also investigates the design of parallel algorithms and is involved in simulations of ionic channels.

Copyright © 2005 John Wiley & Sons, Ltd.